Current Microbiology (2024) 81:404
https://doi.org/10.1007/s00284-024-03908-1

Exploring the Genome-wide Expression Level of the Bacterial Strain Belonging to *Bacillus safensis* (MM19) Against *Phomopsis viticola*

Ragıp Soner Silme[1] · Ömür Baysal[2,3] · Ahmet Can[2] · Yiğit Kürüm[2] · Ahmet Korkut[2] · Kevser Kübra Kırboğa[4] · Agit Çetinkaya[5]

Received: 6 June 2024 / Accepted: 14 September 2024 / Published online: 14 October 2024

Abstract

Rhizobacteria have the ability to compete with pathogenic microorganisms and contribute to plant immunity and defense mechanisms. Their growth and survival in the rhizosphere ensure a biological balance in favor of the host plant. The differential gene expression profiles of *B. safensis* (MM19) revealed significantly increased expression of prominent genes related to thiamine biosynthesis involving various metabolites and enzymes that participate in the suppression of mycelium growth and pathogen inhibition. Correspondingly, the expression of three major genes (HOG1, FUS3, SGI) involved in the virulence of *P. viticola* was assessed using qPCR analysis. HOG1 was the highest expressed gene in the pathogen when it was co-cultivated with MM19. Based on these findings, we performed molecular docking and dynamics analysis to explore the interaction between HOG1 and thiamine, as well as expression network analysis constructed using Cytoscape. The functional genomic data related to thiamine biosynthesis and the corresponding pathways ensure a priming role in the antagonistic behavior of *B. safensis* (MM19) against *P. viticola* as a support for plant immunity.

Introduction

Biocontrol is an eco-friendly approach involving the promotion of plant growth, hormone production or the indirect suppression of plant pathogens, and the induction of plant resistance. Rhizobacteria interact with plants through a range of mechanisms that influence their growth and health. The direct interactions between rhizobacterium and plant pathogens encompass a multifaceted relationship involving competition and antibiosis. These interactions involve the production of various compounds, including antibiotics, cyclic lipoproteins, antimicrobial volatiles, siderophores, and exoenzymes, which collectively contribute to the dynamic interplay among these microorganisms [1, 2].

Bacillus species are able to mitigate disease severity in various economically significant crop species. *Bacillus* spp. are ubiquitous bacteria found in soils that exhibit antagonistic properties against crop pathogens [3]. Some strains secrete antibiotics that can directly inhibit the growth of fungal, oomycete, and bacterial plant pathogens [4]. The genetic traits underlying biocontrol efficiency and regulation that play a role in the suppression of plant pathogen growth have been studied for these bacterial strains based on their ability to produce cell wall-degrading enzymes and antibiotic compounds [2, 5–7]. Other strains of *Bacillus subtilis* also suppress diseases by inducing host defence mechanisms [8]. However, additional functional studies are required to understand the ongoing mode of action related to biocontrol. The genome sequences provide insights into the role of traits and their importance in studies conducted on mutant individuals. In view of gene regulation and subsequent activity,

Ragıp Soner Silme and Ömür Baysal have contributed equally to this work.

✉ Ragıp Soner Silme
rsoner@istanbul.edu.tr

✉ Ömür Baysal
omurbaysal@mu.edu.tr; o.baysal@worc.ac.uk

1 Center for Research and Practice in Biotechnology and Genetic Engineering, Istanbul University, Istanbul, Fatih, Turkey

2 Molecular Microbiology Unit, Department of Molecular Biology and Genetics, Faculty of Science, Muğla Sıtkı Koçman University, Kötekli-Muğla, Turkey

3 Department of Biological Sciences, University of Worcester, Worcester, UK

4 Faculty of Engineering, Department of Bioengineering, Bilecik Seyh Edebali University, Bilecik, Turkey

5 Department of Molecular Biology and Genetics, Gebze Technical University, Kocaeli, Gebze, Turkey

transcriptome analysis is an important tool for combining the effects of different traits. To the best of our knowledge, these types of studies are few, and the available biocontrol agent-pathogen interactions remain unclear.

Bacillus safensis is a Gram-positive and aerobic chemoheterotroph with spore-forming rod bacterium that are resistant to temperatures between 30 and 37 °C [9]. It is also resistant to 10% salinity and pH level of 5–6. In a previous study, a strain of *B. safensis* was shown to be resistant to UV radiation and hydrogen peroxide [10]. *B. safensis* has the potential to enhance plant growth through both direct and indirect mechanisms. This includes the inhibition of fungal pathogens and the reduction of salt-induced stress in plants [11]. Wu et al. [12] found that *B. safensis* strain ZY16 is an endophytic bacterium that can degrade hydrocarbons, produce biosurfactants, tolerate salt, and promote plant growth through IAA production, siderophore synthesis, and phosphate solubilizing activity.

Phomopsis viticola is a serious pathogen of grapevine cultivated in many regions of the world and is known as Phomopsis dead arm disease [13]. Recent research findings have indicated that pruning wounds remain vulnerable to infection for an extended period, with susceptibility persisting for a minimum of three weeks following the pruning process [14]. One of the strategies for grapevine protection against this pathogen is the reduction of *P. viticola* inoculum on canes, both during the vegetative and dormant periods, which also results in protection against fungus distribution [15]. Therefore, chemical applications are traditionally recommended [16].

In the management of Phomopsis dead arm disease, a range of early-season spray treatments, including copper oxychloride, copper oxychloride/sulphur, copper sulphate/lime, folpet, fosetyl-Al + mancozeb, propineb, sulphur and strobilurin-based fungicides, are used [17]. There are no fungicides that are both effective and environment-friendly in suppressing the fungus. Furthermore, the research conducted by Munkvold and Marois revealed that the efficacy of chemicals such as benomyl exhibited a decline in effectiveness two weeks after application [18]. These findings have shown the importance of finding alternative methods that could replace protective pruning and chemical application. There is no data on the biocontrol of *P. viticola* via *B. safensis* treatment. Depending on the abovementioned situation, the importance of a rhizobacterium that can control Phomopsis in terms of biological control becomes evident.

Whole-transcriptome analysis with RNA-seq has opened a new dimension to understand gene regulation and how it changes on account of the interactions between the host and the pathogen, which can shed light on the mechanisms of pathogenicity, host defence, and their interplay under various conditions [19]. Currently, RNA-seq is the major method used in transcriptomics studies, and RNA plays a key role in various cellular processes. Therefore, investigation of the identity, function, and abundance of transcribed RNA molecules (i.e., transcripts) are crucial for understanding cellular behavior. Advances in the field of RNA biology have been mainly driven by the development of novel technologies and methods that allow researchers to study different aspects of transcripts in an increasingly efficient manner. Therefore, we investigated the biocontrol agent-pathogen interaction using RNA-seq analysis (Figs. 1, 2)

This study investigated changes in the transcriptional responses exhibited by the bacterial strain MM19 against *P. viticola*. In this study, we conducted a comprehensive analysis of genome-wide gene expression patterns in *B. safensis* in the presence and absence of *P. viticola*. This investigation was performed to elucidate the microbial responses of

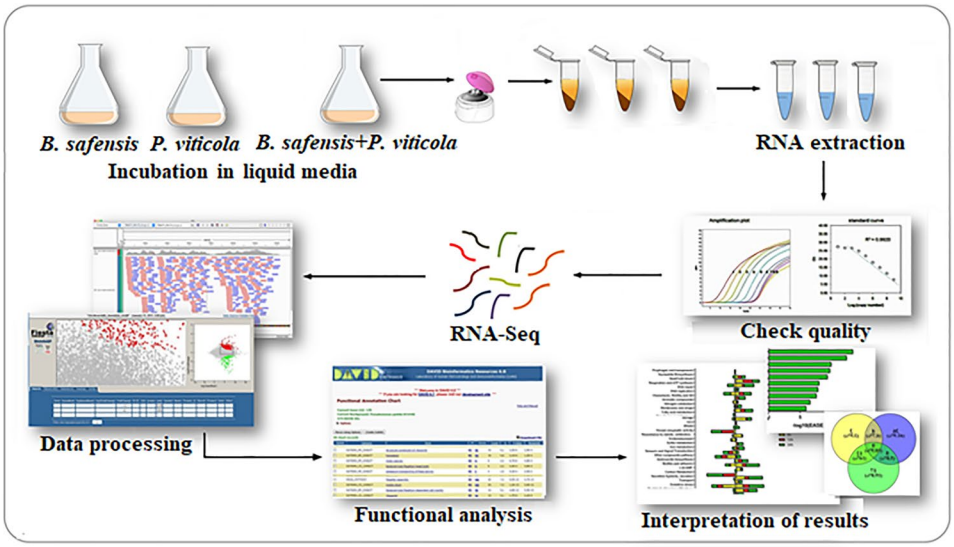

Fig. 1 Workflow of RNA-seq studies. Workflow of the general procedure explained in these protocols. The main wet and in silico steps are summarized in the figure

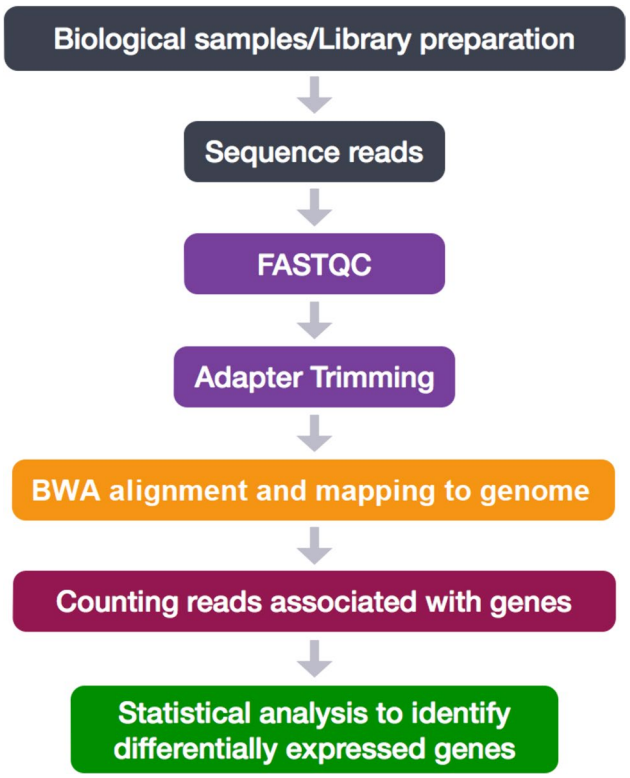

Fig. 2 Overview of the work-chart for assembly of RNA-seq reads for *B. safensis* MM19

B. safensis when coexisting with *P. viticola* under in vitro conditions.

Materials and Methods

Microorganisms and Culture Conditions

The bacterial strain *Bacillus safensis* MM19 (Molecular Microbiology lab, Muğla, 2019) was isolated from soil samples of crude petroleum pollutants contaminated at seashore near petroleum refinements (Aliaga, İzmir, Turkey). The bacterium was cultured on nutrient broth agar (NBA, Merck) and preserved at – 20 °C. The morphological characteristics, Gram reaction, spore formation, and motility of MM19 bacterial strain were examined via microscopic observation. The carbon source preferences of the strain were determined using the Biolog GENIII MicroPlate assay according to the manufacturers' instructions by M. Küsek (Ph.D., Assoc. Prof. at Sütçü İmam University/Kahramanmaraş).

P. viticola samples with diseased grape seedling origin were obtained from the Bornova Plant Protection Research Institute/Izmir. The pathogen was previously identified at the species and genus levels by ITS gene sequence analysis. Subsequently, the pathogen was cultured on potato dextrose agar (PDA, Merck) at 20 °C.

Antagonistic Effects of MM19 in a Single-layer Assay

In vitro experiment, to determine the antibiosis effect, the assay was conducted using single-layer methods. Fungal sections excised from 5-day-old *P. viticola* cultures were placed on fresh PDA medium. When the pathogen mycelium reached the edge of the Petri plates, a sample of the fungi near the center was excised using a cork borer. *P. viticola* culture was then centrally transferred to a culture medium consisting of PDA (*pH* 6.2), then the bacterium was inoculated as two streaks with a 2-cm distance reciprocally at either side of the mycelial plug. Later, the Petri dishes were incubated at 23 °C for one month, and the growth of mycelium was compared to six replicates involving control groups in which only *P. viticola* was present.

The growth of mycelium was measured at 7, 10, and 12 days post-inoculation (dpi) compared with the control group. Radius measurements were obtained from Petri dishes to represent fungal growth in control samples and bacteria inoculated (treated groups). The obtained data were subjected to Student's t-test analysis considering the Bootstrap confidence level using SPSS (IBM SPSS Statistics for Windows, Version 22.0. Armonk, NY: IBM Corp.).

Reciprocal Growth of Microorganisms in Liquid Culture following Interaction and RNA Isolation

For RNA isolation, the optical density (OD) of *B. safensis* depending on colony growth was measured in vitro using single (control) or dual liquid culture systems in which *B. safensis* was replaced alone and interacted with *P. viticola*. To determine whole-expressed genes playing a role in antibiosis, the liquid culture consisted of equal amounts (50/50%) of potato dextrose (PD) and nutrient broth (NB) medium. The fungi obtained from 5-day-old *P. viticola* cultures were excised from PDA medium using a cork borer and released into 15-ml glass bottles containing PD liquid culture. Concomitantly, bacteria were inoculated into liquid culture and allowed to grow until the OD level reached 1.0. Then, two different inoculated liquid cultures containing bacteria and fungi were mixed into a 30 ml Erlenmayer flask and cultured until the common OD level reached 1.0, during which shaking culture required 3.5 h. Then, the RNA extraction procedure given below was followed.

During RNA extraction, the bacterial solution was filtered using sterile Whatman paper to separate the fungal mycelia. Then, the bacterial solution was gently rinsed with the fungicide penconazole (10 µl/15-ml) (100 g/l CAS No: 66246–88-6) for a maximum of 2 min to minimize contamination with fungi in bacterial RNA.

Bacterial RNA Extraction and Sample Preparation for RNA-seq Analysis

Harvested bacterial cells treated with fungicide were subjected to RNA extraction using a GeneJET RNA Purification Kit (K0372, Thermofischer) according to the manufacturer's instructions for extraction of total RNA from bacterial cells. Total RNA was quantified using an ND-1000 spectrophotometer (NanoDrop Technologies, Delaware, USA).

Total RNA was used as the input material for the preparation of RNA samples. Sequencing libraries were constructed using the NEBNext Ultra RNA Library Preparation Kit for Illumina (NEB, USA, Catalog #: E7530L) in accordance with the manufacturer's instructions. Index codes were introduced to associate individual sequences with their respective samples. mRNA was isolated from total RNA using poly-T oligo-affixed magnetic beads. The fragmentation process was conducted by subjecting the RNA to elevated temperatures in the presence of divalent cations and performed within the NEB Next First Strand Synthesis Reaction Buffer (5X). The first strand of complementary DNA (cDNA) was synthesized using a random hexamer primer and M-MuLV reverse transcriptase, which possesses ribonuclease H (RNase H) activity. Synthesis of the second strand of cDNA was performed using DNA polymerase I in conjunction with RNase H. The remaining overhang regions were converted into blunt ends by exonuclease and polymerase enzymatic activities. After adenylation of the 3' ends of the DNA fragments, NEB Next adaptors featuring a hairpin loop structure were ligated to facilitate preparation for hybridization. To selectively isolate cDNA fragments ranging from 370 to 420 base pairs in length, the library fragments were purified using the AMPure XP system (Beverly, USA). Subsequently, 3 µL volume of USER Enzyme (NEB, USA) was applied to the size-selected, adaptor-ligated cDNA, incubated at 37 °C for 15 min, and then subjected to a 5-min incubation at 95 °C before PCR amplification. Following these steps, the polymerase chain reaction (PCR) was performed using Phusion High-Fidelity DNA polymerase along with Universal PCR primers and Index (X) primers. The PCR products were prepared using an AMPure XP system, and the quality of the library was evaluated using the Agilent 5400 system (Agilent, USA). Quantification of the library was achieved through quantitative polymerase chain reaction (QPCR), resulting in a concentration of 1.5 nM. The validated libraries were combined and subjected to sequencing on Illumina platforms (Ficus Bio Co., Ankara-Türkiye), employing paired-end 150 base pair (PE150) sequencing, specifically using the Illumina HiSeq 2500 system. Sequencing depth was determined based on effective library concentration and data quantity.

Table 1 Primer sequences used for qPCR validation

Primers		Sequences
HOG1	Forward	5′ATTCAGGATCCGCAGATGAC3′
	Reverse	5′GCCAGGTCAGCATAATTTCC3′
FUS3	Forward	5′GAAACCACCGAAACCAAAGC3′
	Reverse	5′GTGCCCAGATGTTTTTCCAG3′
SGE1	Forward	5′TTAAACGCTGGACCGATAGC3′
	Reverse	5′CAGTTCGCGATACAGCAGATAG3′

Raw Data and Bioinformatics Analysis

The original fluorescence image files obtained from the Illumina platform are transformed to short reads (raw data) by base calling, and these short reads are recorded in FASTQ format [20], which contains sequence information and corresponding sequencing quality information. Fastp (version 0.23.1) was used to perform basic statistics on the quality of the raw reads [20]. The steps of data processing involve a) discarding paired reads if either read contains adapter contamination, b) discarding paired reads if more than 10% of bases are uncertain in either read, and c) discarding paired reads if the proportion of low-quality (Phred quality < 5) bases is more than 50% in either read.

Sequence artifacts, including reads containing adapter contamination, low-quality nucleotides, and unrecognizable nucleotides (N), undoubtedly set the barrier for reliable bioinformatics analysis. The paired-end reads for each sample were imported into the Galaxy software platform and mapped to the reference genome *Bacillus safensis* (https://www.ncbi.nlm.nih.gov/datasets/genome/GCF_003254445.1/) [21]. FastQ data were subjected to optimized trimmomatic tools (adjusted parameters for MINLEN, LEADING, CROP and HEADCROP) to remove adaptor sequences for fastQC analysis. Then, RNA STAR was used to obtain BAM files from single- and pair-end sequences after MultiQC analysis and then visualized using Tablet (Hutton Institute ver. 1.21.02.08) [22]. The multiple count datasets for multiple samples were retrieved and converted to a single file using feature counts. Then, the data counts were subjected to DeSeq2 analysis using Python (ver. 2023.2) through Sambomics tools to determine upregulated and down-regulated genes and logFc data. The data were submitted to the IDEP platform to visualize the heatmap and other options related to gene counts [23]. To determine WP values corresponding to gene IDs, BLAST analysis was also performed. To annotate the expressed genes, BLASTx searches (E value < 10–3) were performed between nr and unigenes. The BLAST results were imported into the Blast2GO program for further annotation of the unigenes [24]. Genes were attributed

as differentially expressed when the fold change was greater than ± 2 and with an FDR corrected *p*-value of ≤ 0.05.

Gene enrichment analysis was performed using ShinyGO v0.741 [25] based on *Bacillus subtilis* STRINGdb and visualized using SRTplot [26]. Because no specific genomic data were available for *B. safensis* in these analyses tools, we also compared the whole protein expression mapping obtained using the UniProt database with the available data for *B. subtilis*.

Enrichment Gene Interaction Map and Network Analysis

An enrichment map was generated via files derived from RNA-seq outputs using Cytoscape, an open-source and freely accessible plugin designed for network analysis, specifically utilized for the visualization of enriched pathways within a network context. This process involves incorporating elements such as expression profiles, hallmark gene sets, enrichment sets, and parameter specifications such as p values and overlap coefficients [27]. The enrichment map visually represents pathways as a network, where nodes correspond to distinct pathways and are interconnected by edges indicating shared common genes within the related pathways. Moreover, the examination of individual gene interactions pertaining to diverse pathways involves the selection of relevant genes, and subsequently, a network is constructed by annotating these genes through the String Database, utilizing Cytoscape software [28].

qRT-PCR Analysis of Three Selected Major Virulence Genes

The fungal solution was treated with 10 µl Ampicillin (1000 mg/ml) for 15 min to remove the bacterial cells. Harvested fungal mycelia from the liquid culture were used for total RNA extraction using a GeneJET RNA Purification Kit (K0372, Thermofischer) according to the manufacturer's instructions for yeast. Total RNA was measured using spectrophotometry and was used for qRT-PCR analysis.

Due to limited studies on the specific virulence genes of *P. viticola*, we carried out qRT-PCR analysis from the extracted RNA of fungi, which was concomitantly obtained from liquid culture when bacteria and fungi grow together, and followed the expression level of the HOG1, FUS3, and SGE1 genes of *P. viticola* considering a previous study carried out on *P. longicolla,* which is in the same genus [29] (Table 1).

qRT-PCR analysis was performed for the three major selected genes and validated as follows: The first cDNA strand was prepared using the iScript™ cDNA synthesis kit (Bio-Rad). qRT-PCR was performed using the SsoFast™ EvaGreen® supermix kit (Bio-Rad) in which each 20 µl of the RT-PCR reaction mixture contained 25 ng of cDNA (equivalent of 25 ng RNA) and 0.125 µM of each primer. Three genes with non-altered expression (Actin) were selected as reference genes (AhActin- F-5′CTGAAAGAT TCCGATGCCCTGA3′, AhActin- R-5′AACCACCACTCA AGACAATGTTACCA3′) [30]. Forward and reverse primer pairs (Table 1) for each gene were designed using Primer3 software with an amplicon size of 90–200 bp (Supplementary Data S1) [31]. Real-time quantitative PCR was performed using the MyiQ™5 Real-Time PCR Detection System (Bio-Rad) with the following thermal cycle parameters: initial activation 100 at 95 °C for 30 s, followed by 40 cycles of denaturation at 95 °C for 5 s and annealing/extension at 58–60 °C for 10 s. Each run was followed by melt curve analysis. A standard curve was prepared for each gene using a cDNA sample. The relative expression of differentially altered genes was analysed using a free tool (https://goldbio.com/qpcr-and-rtqpcr-analysis-tool) according to Pfaffl [32].

Molecular Docking-based Virtual Screening for Protein–Ligand Interactions

The experimental X-ray diffraction structure of HOG1 (high-osmolarity glycerol 1), with its corresponding Protein Data Bank (PDB) identification number 1WFC, was obtained from the Research Collaboratory for Structural Bioinformatics (RCSB) PDB website [33, 34]. The missing residues from the structure were added via PyMol's builder plugin (open-source v2.5.0), and loop regions where the residues were added, which were refined using MODELLER (v10.1) [35–37]. Subsequently, the structure was subjected to a purification process, in which all heteroatoms were removed, except for the atoms associated with cofactors. In addition, polar hydrogen atoms were introduced where deemed essential, and Kollman charges were calculated [38]. A grid box measuring 24 Å in the X-axis, 24.8 Å in the Y-axis, and 37.5 Å in the Z-axis was computed to encapsulate the active site of the 1WFC structure. Virtual screening was performed using the HOG1 structural model, evaluating its interaction with the thiamine ligand within a pre-determined grid box. Screening was conducted with an exhaustiveness level of 64 using AutoDock Vina (v1.1.2) [39]. The ligands exhibiting the highest affinity scores were subsequently selected using the same configuration.

Protein–Ligand Interaction Profiling

The best dock pose of the ligand was loaded with HOG1 to PyMol, and all residues within 4 Å from the lead compound were visualized (i.e., all potential, hydrophobic interactions, hydrogen bonds, and ionic interactions) and evaluated. The manually predicted bonds were also cross-validated using the TU Dresden's Protein–Ligand Interaction Profiler (PLIP)

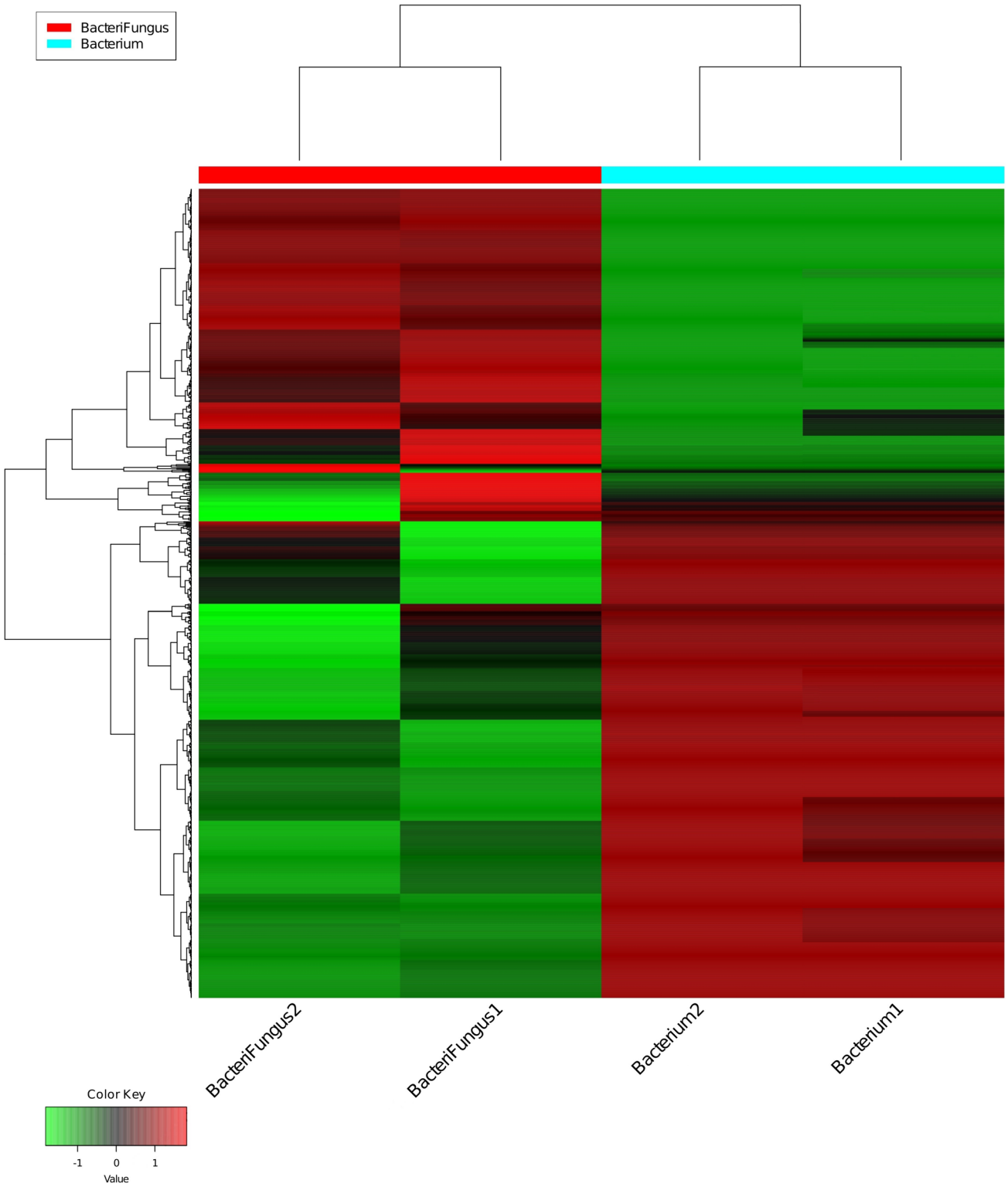

Fig. 3 Transcriptomic data obtained from the flasks of bacteria-fungi interaction groups and bacteria alone. Transcriptional levels of the relevant genes in *Bacillus safensis* MM19 are shown as a heat map, based on the ranking of expression intensity in the whole genome. The color of each square represents the strength of gene transcription

webserver, and only overlapping interactions were considered [40].

Molecular Dynamics Analysis

Docking research often neglects the dynamic nature of proteins. To gain a comprehensive understanding of binding configurations and assess system stability, it is critical to perform molecular dynamics (MD) assessments. Such simulations offer computational approaches for exploring the temporal dynamics of molecular arrangements [41, 42]. In our investigation, we used the Desmond component of Maestro's academic edition to execute MD assessments [43]. This enabled us to scrutinize system interactions, structural alterations, and overall behaviors between the ligand and protein. This investigation explored the stability and dynamic characteristics of a complex involving a protein and the ligand. We examined the protein (PDB ID: 1WFC) along with thiamine as the ligand under simulation conditions. Our objective was to understand how ligands affect protein stability and identify the protein sectors that exhibit the most significant variations. The simulations were conducted in an NPT ensemble at 300 K for 100 ns. The OPLS-AA force field was employed for the complex, and the ligand parameters were generated using Maestro's LigPrep module [43]. The NPT ensemble is a form of MD simulation that accounts for the number of particles, pressure, and temperature within the system. This allows for a constant volume and temperature setting in which the pressure can vary, making it useful for studying systems in solution-based and life-like simulation settings. During the simulation, we tracked the root mean square deviation (RMSD) of both protein and ligand. We also measured the protein's RMSF to detect localized alterations along its chain. The RMSF metrics for individual residues were observed throughout the simulation, allowing us to identify the most variable regions within the protein structure. In addition, we mapped out contacts between the ligand and protein to identify specific residues involved in ligand binding, marking these areas with green vertical lines for easier visualization. We also continuously observed the protein's secondary structure, which reflects local folding patterns such as alpha helices and beta sheets. These structures are critical for protein functionality, and their alterations can influence protein activity. Finally, we documented the existence of counterions and the concentration of salts in the solvent, which can significantly affect the system's dynamics. To summarize, our MD simulation provided valuable insights into the stability and dynamics of a protein–ligand complex under specific conditions, including monitoring the RMSD and RMSF values, the identification of residues interacting with the ligand, observations of the protein's secondary structure, and recording of counterions and salt concentrations in the solvent.

Results and Discussion

Identification of MM19 and its Antagonistic Activity Using Single-layer Assay

The Biolog GEN III results indicated that the bacterial strain belonged to *Bacillus safensis* genus (Supplementary Fig. S1). Further analysis was carried out considering these results (Supplementary Table S1). A significant decrease in the radial expansion of *P. viticola* was observed upon the introduction of *B. safensis* MM19 from day 7 onward, and this inhibitory effect persisted throughout the entire experimental period (Supplementary Fig. S2, Supplementary Table S2).

Transcriptome Profiling of *B. safensis* after the Interaction with *P. viticola*

The obtained RNA-seq data were deposited in the DDBJ Sequence Read Archive at the DNA Data Bank of Japan (http://trace.ddbj.nig.ac.jp/dra) under accession number SAMD00731600 (BioProject; PRJDB17356). The analysis generated 1.4 million raw reads for each sample, of which 80.0% were correctly mapped to the *B. safensis* reference genome of NCBI, which contained 3996 annotated genes. The mean CPM and k-values for the samples are shown in supplementary data S2. In this study, after the *P. viticola* interaction, the genes showed twofold increase in up-regulation and down-regulation (Table 1) (Supplementary Fig. S3). Of 1004 genes, 527 were up-regulated and 477 were down-regulated (Fig. 3, Fig. 4 and Supplementary Data S2). RNA-seq analysis identified 3398 genes of bacteria involved in this interaction with fungi when growing together in liquid culture.

Transcriptomic data obtained from bacteria show changes up- and down-regulation. The expression profile has changed depending on stress conditions in bacteria and varies in RNA samples obtained from bacteria-fungi interactions and bacteria alone groups. The expressed genes demonstrated differentiation. The genes up-regulated in bacterial growth in liquid culture medium showed down-regulation when the bacteria growth with *P. viticola*, and vice versa, the genes that were down-regulated before showed up-regulation ascending when the bacteria growth with *P. viticola* (Fig. 3, Fig. 4). The S-adenosylmethionine decarboxylase genes were highly up-regulated (Fig. 4). In a previous study, proteomics analysis indicated the up-regulation of S-adenosylmethionine (SAM)-dependent methyltransferases in a bacterial strain belonging to *Bacillus* species (EU07)

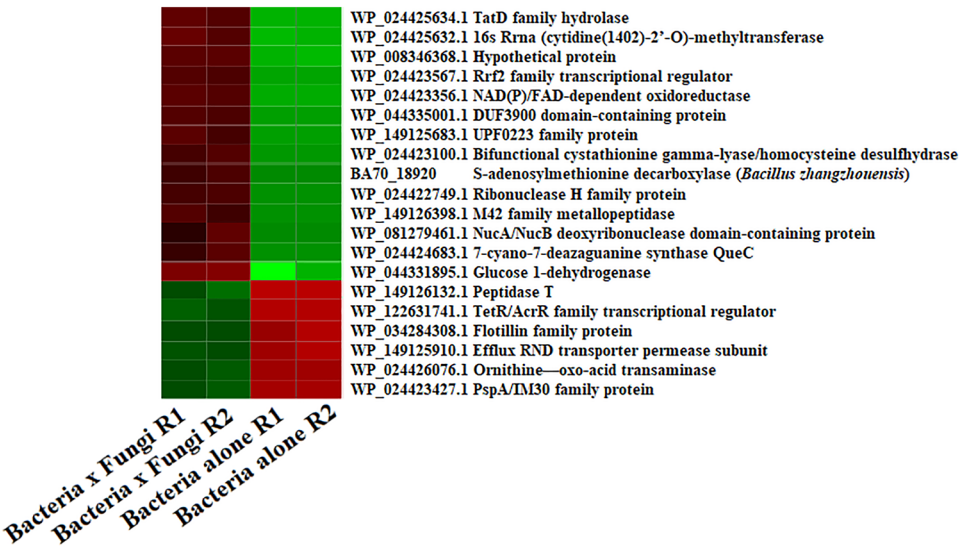

Fig. 4 The most variable top 20 genes in bacterial transcription during the bacteria-fungi interaction according to logFC values

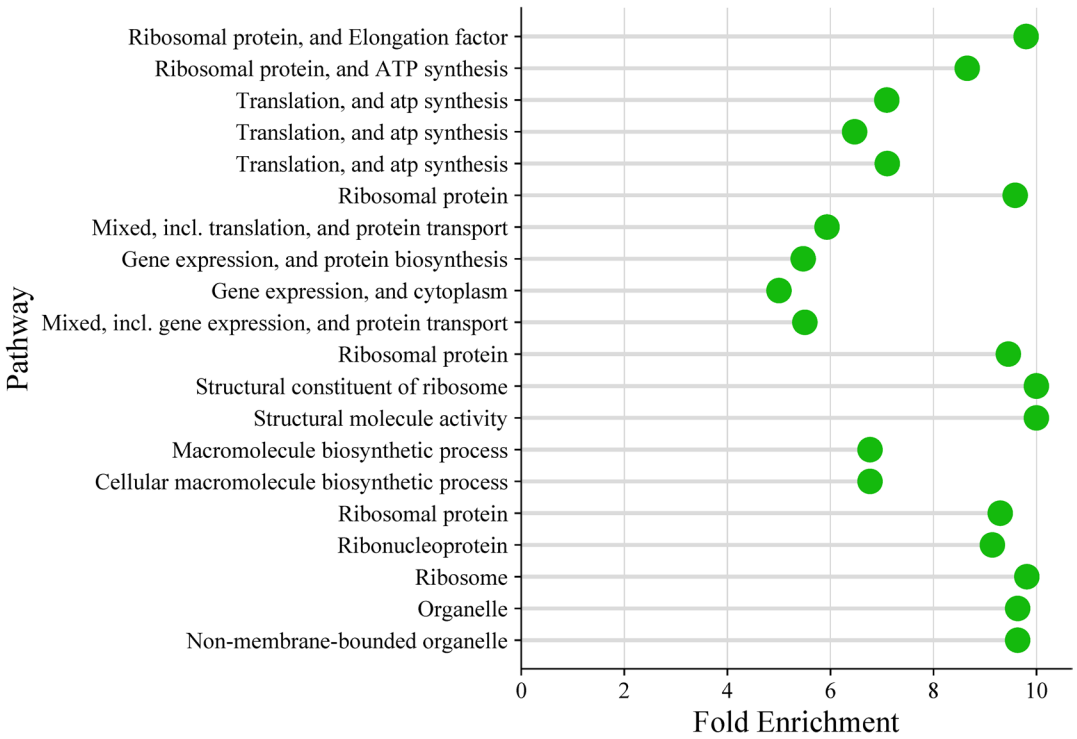

Fig. 5 The chart shows a hierarchical clustering tree summarizing the correlation among significant pathways listed in the enrichment table. Pathways with many shared genes are clustered together. Bigger dots indicate more significant P-values

(later identified as *Bacillus velezensis*) when it encountered *Fusarium oxysporum* radicis-*lycopersici* [5]. Correspondingly, in the present study, RNA expression analysis indicated a decrease in S-adenosylmethionine decarboxylase, which converts 1-aminocyclopropane-1-carboxylate (ACC) synthase into S-adenosylmethionine (AdoMet), when MM19 was encountered in *P. viticola* (Fig. 4). This result could be linked with the substitution of S-adenosylmethionine with SAM-dependent methyltransferases, which could allow bacteria to utilize this pathway as an alternative response to *P. viticola*, which could be linked to quorum sensing and common virulence behavior of the bacteria toward the target pathogen. It is also noteworthy that these genes could also be involved in riboswitches, which are highly

Table 2 Genes shown in italics letters were grouped by functional categories that were defined by high-level GO terms according to RNAseq output showing up-down-regulations

High level GO category	Genes
Cellular process	*spoVG rpsJ rplW rpsS rplV rpsC rplP rpsN1 rpmD infA rpmJ rpsM rpsK rpoA rplQ rplM aroK recR sspK rpmF mraY rpoZ rpmB ylxS rbfA ymdA ypsB folE nusB rpsU rpmA yshA rpmI smpB fabZ atpC upp rpmE2*
Metabolic process	*rpsJ rplW rpsS rplV rpsC rplP rpsN1 rpmD infA rpmJ rpsM rpsK rpoA rplQ rplM aroK recR rpmF mraY rpoZ rpmB rbfA ymdA folE nusB rpsU rpmA rpmI smpB fabZ atpC upp rpmE2*
Cellular metabolic process	*rpsJ rplW rpsS rplV rpsC rplP rpsN1 rpmD infA rpmJ rpsM rpsK rpoA rplQ rplM aroK recR rpmF mraY rpoZ rpmB rbfA ymdA folE nusB rpsU rpmA rpmI smpB fabZ atpC upp rpmE2*
Organic substance metabolic process	*rpsJ rplW rpsS rplV rpsC rplP rpsN1 rpmD infA rpmJ rpsM rpsK rpoA rplQ rplM aroK recR rpmF mraY rpoZ rpmB rbfA ymdA folE nusB rpsU rpmA rpmI smpB fabZ atpC upp rpmE2*
Nitrogen compound metabolic process	*rpsJ rplW rpsS rplV rpsC rplP rpsN1 rpmD infA rpmJ rpsM rpsK rpoA rplQ rplM aroK recR rpmF mraY rpoZ rpmB rbfA ymdA folE nusB rpsU rpmA rpmI smpB atpC upp rpmE2*
Primary metabolic process	*rpsJ rplW rpsS rplV rpsC rplP rpsN1 rpmD infA rpmJ rpsM rpsK rpoA rplQ rplM aroK recR rpmF rpoZ rpmB rbfA ymdA nusB rpsU rpmA rpmI smpB fabZ atpC upp rpmE2*
Biosynthetic process	*rpsJ rplW rpsS rplV rpsC rplP rpsN1 rpmD infA rpmJ rpsM rpsK rpoA rplQ rplM aroK rpmF mraY rpoZ rpmB folE nusB rpsU rpmA rpmI smpB fabZ atpC upp rpmE2*
Intracellular	*rpsJ rplW rpsS rplV rpsC rplP rpsN1 rpmD infA rpmJ rpsM rpsK rplQ rplM aroK rpmF rpmB ylxS rbfA ypsB rpsU rpmA yshA rpmI smpB fabZ atpC rpmE2*
Binding	*rpsJ rplW rpsS rplV rpsC rplP rpsN1 infA rpsM rpsK rpoA aroK recR rpoZ ymdA folE nusB smpB atpC upp rpmE2*
Organic cyclic compound binding	*rpsJ rplW rpsS rplV rpsC rplP rpsN1 infA rpsM rpsK rpoA aroK recR rpoZ ymdA folE nusB smpB atpC upp rpmE2*
Heterocyclic compound binding	*rpsJ rplW rpsS rplV rpsC rplP rpsN1 infA rpsM rpsK rpoA aroK recR rpoZ ymdA folE nusB smpB atpC upp rpmE2*
Structural molecule activity	*rpsJ rplW rpsS rplV rpsC rplP rpsN1 rpmD rpmJ rpsM rpsK rplQ rplM rpmF rpmB rpsU rpmA rpmI rpmE2*
Organelle	*rpsJ rplW rpsS rplV rpsC rplP rpsN1 rpmD rpmJ rpsM rpsK rplQ rplM rpmF rpmB rpsU rpmA rpmI rpmE2*
Structural constituent of ribosome	*rpsJ rplW rpsS rplV rpsC rplP rpsN1 rpmD rpmJ rpsM rpsK rplQ rplM rpmF rpmB rpsU rpmA rpmI rpmE2*
Non-membrane-bounded organelle	*rpsJ rplW rpsS rplV rpsC rplP rpsN1 rpmD rpmJ rpsM rpsK rplQ rplM rpmF rpmB rpsU rpmA rpmI rpmE2*
Intracellular organelle	*rpsJ rplW rpsS rplV rpsC rplP rpsN1 rpmD rpmJ rpsM rpsK rplQ rplM rpmF rpmB rpsU rpmA rpmI rpmE2*
Catalytic activity	*rpoA aroK mraY rpoZ ymdA folE fabZ atpC upp*
Ion binding	*rpsN1 aroK recR folE atpC upp rpmE2*
Membrane	*yebE mraY ymdA yneF yshA atpC*
Plasma membrane	*yebE mraY ymdA yneF yshA atpC*
Transferase activity	*rpoA aroK mraY rpoZ fabZ upp*
Cell periphery	*yebE mraY ymdA yneF yshA atpC*
Protein-containing complex	*rpsS rplV rpmD rpmF atpC*
Regulation of biological process	*infA mraY ymdA ypsB nusB*
Biological regulation	*infA mraY ymdA ypsB nusB*
Cellular component organization or biogenesis	*spoVG mraY ylxS rbfA yshA*
Cellular component biogenesis	*spoVG mraY ylxS rbfA yshA*
Intrinsic component of membrane	*yebE mraY ymdA yneF*
Small molecule binding	*aroK folE atpC upp*
Carbohydrate derivative binding	*aroK folE atpC upp*

Table 2 (continued)

High level GO category	Genes
Ribonucleoprotein complex	*rpsS rplV rpmD rpmF*
Cellular component organization	*spoVG mraY yshA*
Regulation of metabolic process	*infA ymdA nusB*
Reproduction	*spoVG sspK*
Developmental process	*spoVG sspK*
Anatomical structure morphogenesis	*spoVG sspK*
Hydrolase activity	*ymdA folE*
Asexual reproduction	*spoVG sspK*
Cell cycle process	*spoVG yshA*
Anatomical structure formation involved in morphogenesis	*spoVG sspK*
Anatomical structure development	*spoVG sspK*
Regulation of developmental process	*mraY ypsB*
Regulation of cellular process	*infA nusB*
Regulation of biological quality	*mraY ypsB*
Transporter activity	*atpC*
Translation regulator activity	*infA*
Response to stimulus	*recR*
Localization	*atpC*
Protein binding	*rpoA*
Response to stress	*recR*
Catabolic process	*ymdA*
Lyase activity	*fabZ*
Ligase activity	*atpC*
Transmembrane transporter activity	*atpC*
Intracellular immature spore	*sspK*
Protein-containing complex binding	*infA*
Negative regulation of biological process	*ymdA*
Establishment of localization	*atpC*
Cellular response to stimulus	*recR*
Cell wall organization or biogenesis	*mraY*
Translation regulator activity, nucleic acid binding	*infA*
Membrane protein complex	*atpC*

conserved metabolite-sensing noncoding RNAs responsible for the regulation of gene expression. They are mostly found in the untranslated regions of mRNAs and can bind directly to small-molecule metabolites, thereby regulating the expression of metabolic-related genes [44]. Riboswitches are signaling molecules that sense various cellular metabolites which alter mRNA transcription profile when they reach the ribosome owing to polycistronic structure of translation in prokaryotes. These metabolites include coenzymes, amino acids, metal ions, and nucleobases [45]. The thiamin diphosphate riboswitch is one of the most widespread riboswitches. Members of this class regulate the expression of genes involved in the biosynthesis, salvage, and transport of thiamin and its precursors [46, 47]. Studies by Schyns et al. [48] on *Bacillus subtilis* confirmed that the mechanism of thiamine gene regulation is controlled via riboswitch. The RNA analysis results showed that ribosomal protein translation was significantly increased and that energy consumption increased with ATP synthesis (Fig. 5).

The prominent genes are ranked according to their degree of importance in the interaction between bacteria and fungi listed in Table 2, and they are separated by functional groups. These results indicate which genes of the bacterium that encounters the fungus respond at transcriptional level to biotic stress. Findings regarding cellular metabolism illustrated that the response of MM19 to *P. viticola* increased

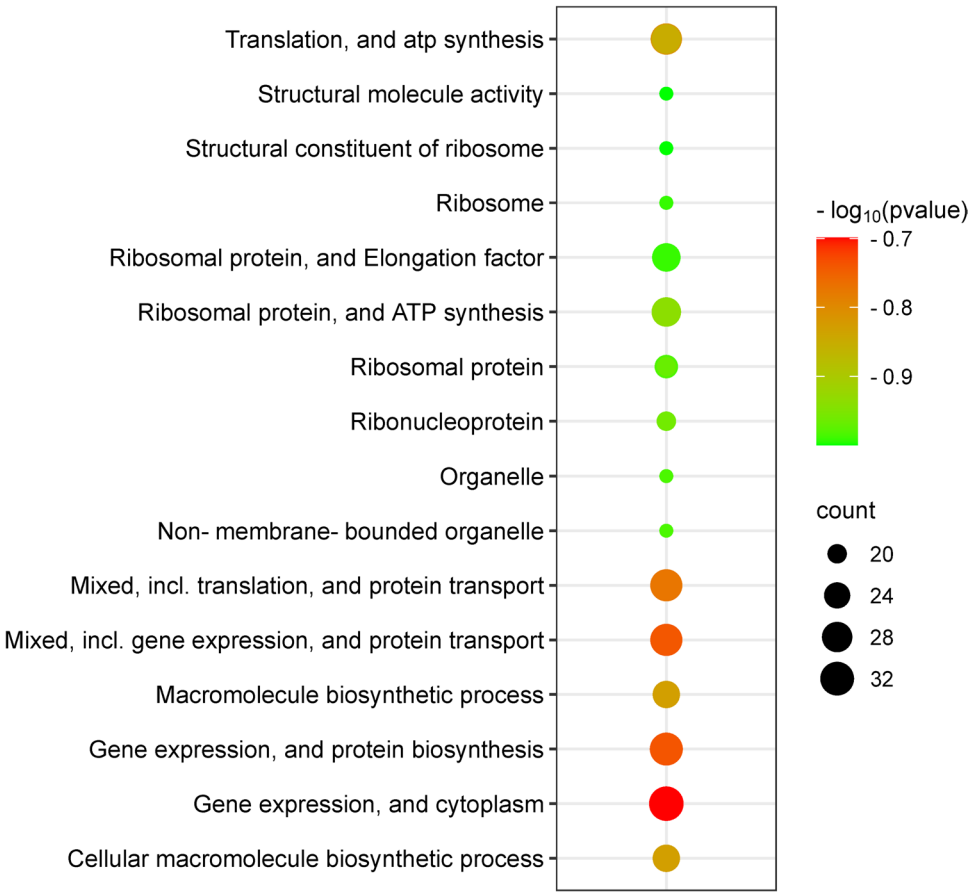

Fig. 6 The illustration shows gene enrichment analysis related to cell metabolism pathways depending on RNA-seq analysis counts that reveals up-regulated or down-regulated genes during bacteria and fungi interaction

the gene expression level with related many metabolic bioprocesses, which specifically resulted in enhanced protein synthesis (Fig. 6). We observed that ribosomal proteins and transcriptional processes tended to ascend with biotic stress. Considering the genes given in Table 2, common expressions occurring in the genes of bacteria can be observed. Based on this finding, we could use these data as a parametric measurement for qPCR-based methods to understand antagonistic behavior involving responsible genes for further studies.

There is no genomic database for comparing the expressed specific genes in *B. safensis* for gene enrichment analysis in ShinyGO; therefore, we used *B. subtilis* strain 168 as a reference. The p values of the biosynthesis and metabolic events that stand out in the enrichment analysis are listed in the appendix, as visualized in ShinyGO (Supplementary Data S3, Supplementary Data S4). Since the bacterium varies the regulation of several genes depending on their functions, it is more valuable to interpret the clustering of these genes. Gene enrichment analysis revealed the major metabolic pathways of up-regulated or down-regulated genes during bacteria-fungi interactions (Fig. 7). In this analysis, the oxidoreductase activity acting on the CH-NH_2 group of donors, oxygen as a receptor, FAD-dependent oxidoreductase, and FAD-binding processes play major roles in total metabolic processes. In addition, most genes involved in thiamine metabolic pathways were highly expressed during interactions with fungi (Fig. 7).

Specifically, oxidoreductases consist of several different enzymes, such as peroxidase, reductase, dehydrogenase, oxidase, oxygenase, and hydroxylase. It participates in both anaerobic and aerobic metabolism [49]. Oxidoreductases catalyze the oxidation and reduction reactions within cells. However, it often needs cofactors such as nicotinamide adenine dinucleotides (e.g., NAD^+/NADH) and flavines (e.g., FAD/$FADH_2$) in the reactions. In fact, nicotinamide adenine dinucleotides are require by nearly 80% of oxidoreductases. Several NAD (H) regeneration systems have been developed; the most widely used is formate-formate dehydrogenase (FDH) system [50]. In light of these findings, our RNA-seq data indicated that when bacteria encountered fungi, their oxidation metabolism increased more than before.

Diaporthe (*Phomopsis*) fungi generate natural products such as pyrones, polyketides, alkaloids, and terpenoids. Most natural products have antibacterial, anti-inflammatory, and/or cytotoxic activities [51]. One of these products is Trichothecene which is one of the major classes of mycotoxins, has a common 12, 13-epoxytrichothec-9-ene

Fig. 7 The illustration shows gene enrichment analysis related to metabolic pathways depending on RNA-seq analysis counts that reveals up-regulated or down-regulated genes during bacteria and fungi interaction

structure in which the epoxy group is the active site leading to oxidative radical formation [52, 53]. The oxidoreductase-dependent metabolic pathways could be overexpressed to overcome the oxidative radicals secreted by fungi (Fig. 7). In a previous study, Afsharmanesh et al. [54] found that oxidoreductase from *B. subtilis* UTB1, which can degrade aflatoxins that are highly toxic and hazardous secondary metabolites produced by a specific strain of *Aspergillus* species, e.g., *Aspergillus flavus* and *Aspergillus parasiticus*. Their study indicated that oxidoreductase successfully degrades aflatoxin and reduces the growth of fungal biomass. Therefore, bacterial oxidoreductases of MM19 can play a major role for degradation of the toxic metabolites produced by the fungus.

Thiamine (vitamin B1) is an essential cofactor in the carbohydrate metabolism involving biosynthesis and degradation of branched-chain amino acids [55–57]. Therefore, the availability of thiamine has a key effect on the growth of many organisms, e.g., *Xanthomonas oryzae* pv. *oryzae* [58] and *Listeria monocytogenes* [59]. Noteworthy, the studies of Liu et al. [60] indicated that thiamine is essential for the virulence and survival of *Pseudomonas syringae* pv. *tomato*; therefore, we can suggest that the transcriptional activation of thiamine-related genes in MM19 plays a major role in the challenge during the *P. viticola* interaction. Moreover, there are no data on the antifungal effects of the thiamine derivatives. From this perspective, we have investigated the docking simulation of a virulence protein of *P. viticola*, HOG1 and thiamine interaction.

Enrichment Gene Interaction Map and Network Analysis

The enrichment gene interaction map and network analysis results linked to the metabolic map of pathways responsible for thiamine biosynthesis are presented in Fig. 8. The metabolic network was constructed based on KEGG pathway analysis using Cytoscape (Supplementary Data S5; S6; S7; S8, Supplementary Fig. S4; S5; S6). Four modules were partitioned according to their functions, respectively. The illustration shows different metabolic modules: 1, Purine pathway, 2, Cysteine and Methionine pathway, 3, Glycolysis/Gluconeogenesis pathway module, and 4, Phenylalanine, Glycine pathway.

qRT-PCR Analysis on Selected 3 Major Genes Responsible for Virulence

Even though we tried obtaining RNA samples of *P. viticola* through liquid dual culture, we were not able to supply sufficient uncontaminated RNA quantities without bacterial DNA contamination, which was necessary for library

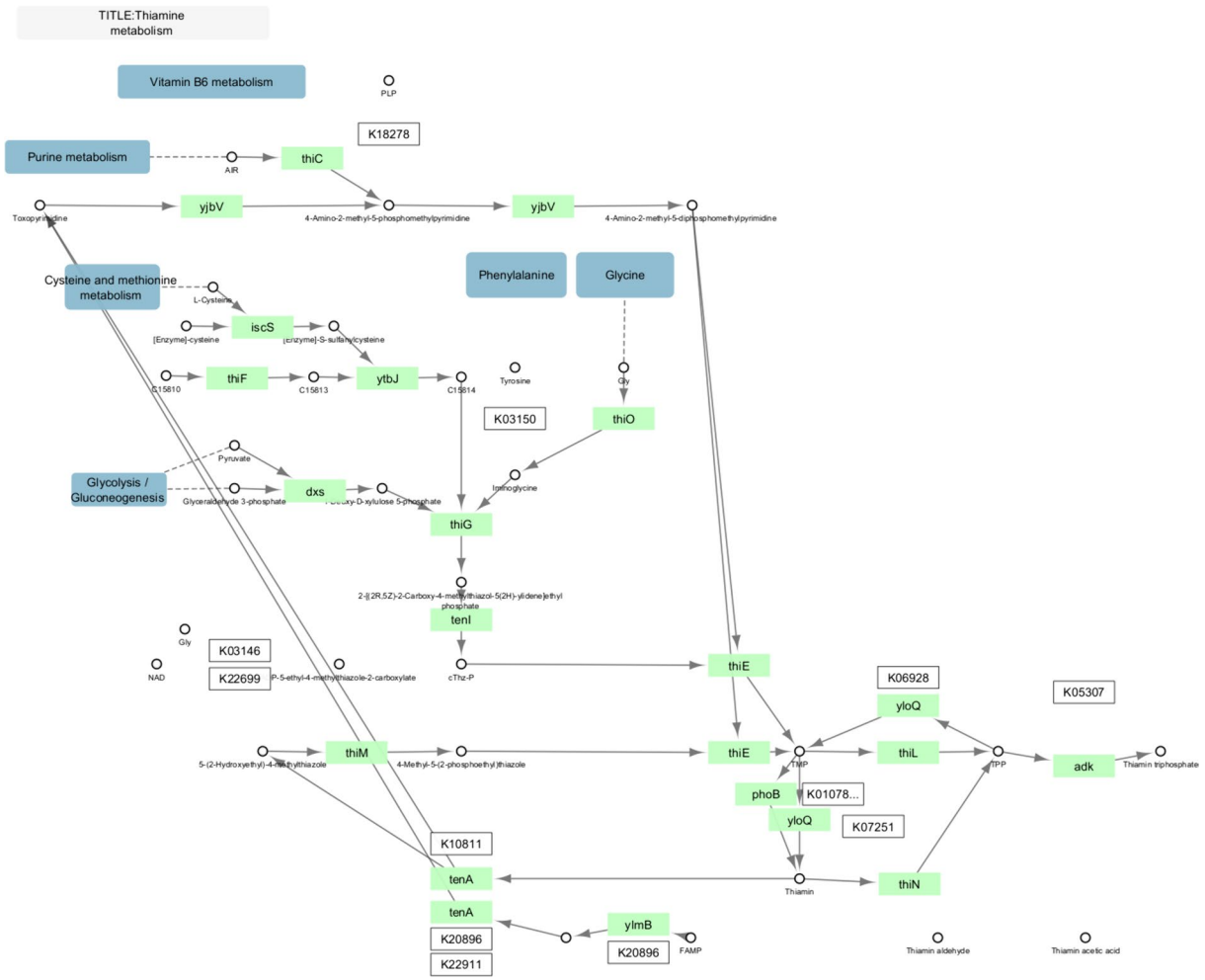

Fig. 8 The illustration shows expression analysis of networks using Cytoscape. The network was constructed considering major variable genes (light green) obtained with RNA-seq analysis

construction of *P. viticola*. Therefore, we could not obtain raw RNA-seq data from fungi although we tried. Instead of RNA-seq, we selected 3 major genes playing a role in the virulence of *Phomopsis longicolla,* which had the most genetically close and available corresponding genes of *P. viticola* [29].

In the qPCR experiments conducted with 4 replicates, the higher expression of HOG1 than the others showed that the interaction of HOG1 with thiamine had a much more considerable case that should be focused on terms of pathogenic growth inhibition by antagonistic bacteria (Fig. 9) (Supplementary Data S9).

Molecular Docking-based Virtual Screening for Protein–Ligand Interactions

The process of virtual screening assessed the ligand's (thiamine) affinity to HOG1, with a specific criterion set at a binding energy threshold ≥ -6.5 kcal/mol. This stringent threshold is indicative of substantial binding strength and the potential for effective ligand-mediated inhibition of the target protein.

Protein–Ligand Interaction Profiling

The interaction between the HOG1 catalytic site with the divalent cation and thiamine (as shown in Fig. 10, Supplementary Data S10) was closely analyzed and visualized. Figure 10A illustrates the comprehensive depiction of potential hydrophobic interactions and hydrogen bonds established between individual residues and the lead compound within the active site of HOG1. Additionally, the interacting residues originating from the thiamine backbone are meticulously expanded to enhance the visualization of the interacting atoms.

Fold gene expression = 2^-(ΔΔCt)		
FUS3	**HOG1**	**SGE1**
2.31	2.43	2.41
2.75	2.46	2.97
2.17	**3.14***	2.57
2.69	**10.77***	2.13

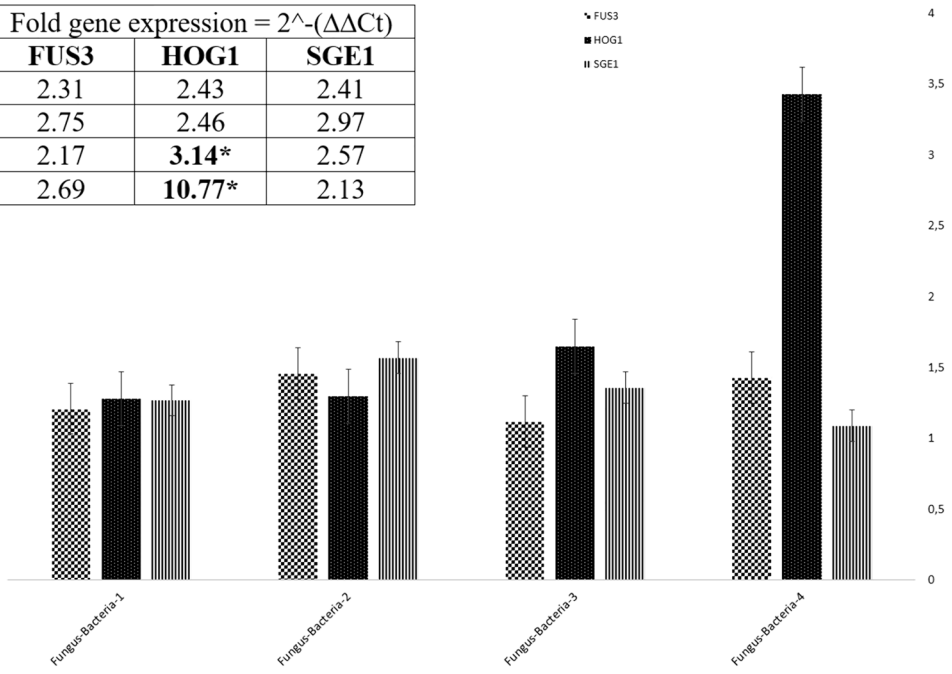

Fig. 9 qPCR validation of selected differentially expressed genes with four replicates. The fold gene expression is given as $2^{-(\Delta\Delta Ct)}$ value compared to housekeeping gene ß-Actin

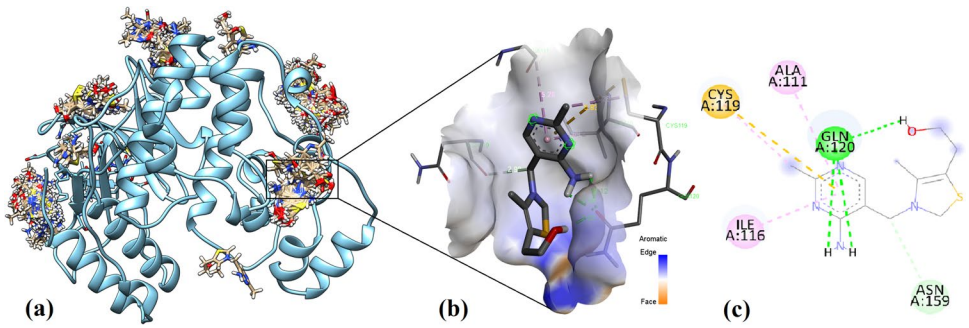

Fig. 10 **a** The complete docking conformation of thiamine (depicted in blue and red) with the transmembrane domain of HOG1, characterized by helical structures, was investigated, focusing multiple thiamine compound binding events on the target protein. The highest binding energy between HOG1 (receptor) and thiamine (ligand) and its coordinates on receptor shown in **b** 3D and **c** 2D

Molecular Dynamics Analysis

The stability of the interaction between HOG1 and thiamine was systematically investigated by simulating 100 ns molecular dynamics (Fig. 11). The RMSD values were employed to assess the equilibrium attainment within the simulation and to discern any notable conformational alterations. Residues 50–60 of the protein are the most fluctuating regions and are effective for ligand binding. The simulation did not exhibit significant alterations in the secondary structure of the protein over its simulation. The protein–ligand RMSD values indicated that the protein and ligand were stable throughout the simulation. The RMSD value varied between 3.2 and 5.6. The RMSD value of the ligand indicates that it fluctuates more throughout the simulation. The RMSD value ranges between 1 Å and 4 Å. The protein jumped around 50 ns. These findings suggest that the ligand has switched to an alternative binding mode. Therefore, the stability of the ligand could have decreased at this point. In conclusion, our MD results showed that the protein and ligand remain stable throughout the simulation, but the ligand switched to different binding modes at various points. This could affect the binding stability of the ligand. In the ligand RMSF graph, the ligand atoms fluctuate in different ways (Supplementary Data S11). Atom number 17 had the highest RMSF value. This atom could play an essential role in the interaction of the ligand with the protein. Additionally, the RMSF value of the ligand varied between 1 and 4 Å (Fig. 12A). The most robust interaction between the protein and ligand was observed with the ASP residue. This relic has a percentage value of 100%. This signifies that this residue is in constant contact with the ligand. This residue could play an essential

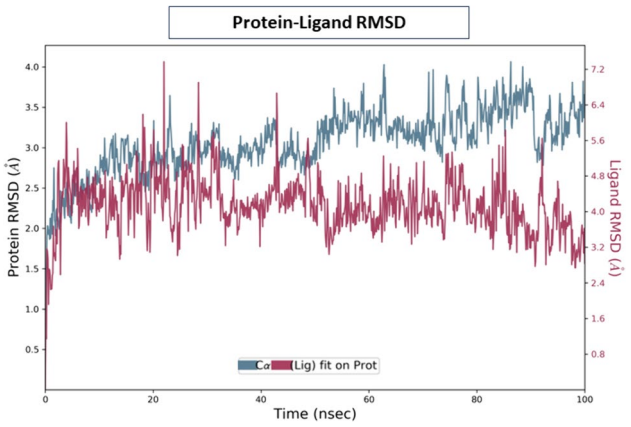

Fig. 11 HOG1 and thiamine simulations were conducted with reference to the initial frame throughout the entire 100 ns production simulation. The cyan line in the graph depicts the trajectory of HOG1 motion. Notably, reduced variability along the Y-axis indicates a lesser degree of deviation from its initial docked position. The red line in the plot represents the root mean square deviation (RMS) of the thiamine backbone, illustrating the displacement of HOG1 during the course of the simulation

role in binding the ligand to the active site of the protein. In Fig. 12B (contacts), there were also weaker interactions between the protein and the ligand. These were those with percentage values lower than 50%. These interactions mean that the ligand temporarily comes into contact with different regions of the protein and can affect its binding stability of the ligand (Supplementary Data S11).

HOG1 is a mitogen-activated protein kinase that plays major roles in fungal cell growth. Mitogen-activated protein kinases are eukaryotic serine-threonine kinases that mediate vital intracellular programs such as proliferation, differentiation, survival, and apoptosis [61]. Studies on *Saccharomyces cerevisiae* by Brewster and Gustin [62] revealed HOG1 as a central signaling mediator during osmoregulation. Due to the signaling specificity properties of kinases involving response and substrate specificity behavior, HOG1 and FUS3 have been attributed as regulator proteins responsible for protein–protein interaction and cell recognition [63]. In light of our findings, it can be presumed that bacteria targeted these two specific kinases through emitted effectors to diminish the pathogenic behavior of *P. viticola*. The bacteria's thiamine production could be linked to HOG1, which results in impairment of the mitogen kinase activated protein responsible for the signal communication of the cell wall. Targeting this protein could be the antagonistic strategy peculiar to the bacterium in order to distract the pathogen behavior in purpose of diminishing its signal transduction which causes specific mRNA transcription that leads to biosynthesis of metabolites. Hence, as described by Siemieniuk et al. [64], thiamine antivitamins could be considered as antifungal agents which suggests such new thiamine derivatives targeting HOG1 can also be employed and tested against *P. viticola* as a pathogen growth inhibitor.

Correspondingly, independent studies revealed that thiamine triphosphate acts as a signaling molecule in the adaptation of bacteria to stress conditions [65]. Adenosine thiamine triphosphate has been suggested to have a role in the response to abiotic stress [66]. Moreover, adenosine thiamine triphosphate is known to be a regulator for the activity of membrane adenosine thiamine triphosphate transporter [67] and poly(ADP-ribose) polymerase-1 [68]. Given that MM19 expressed higher levels of the genes responsible for thiamine biosynthesis (Fig. 7), the prominent property of the bacteria could be linked to its inhibitory effect against pathogenic fungi.

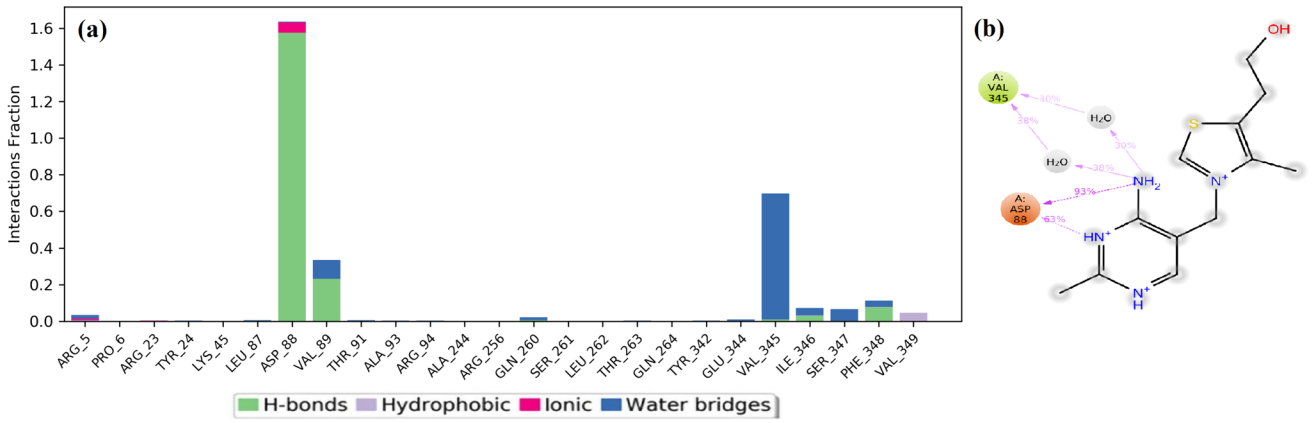

Fig. 12 **a** The histogram illustrating the occurrences of protein–ligand contact along the molecular trajectory is presented. **b** The structural configuration of the protein–ligand complex system was derived through a molecular dynamics simulation, specifically focusing on the two-dimensional interaction mode. Notably, hydrogen bonds, salt bridges, and π-cation interactions are, respectively, delineated in the visual representation using green, pink, and dark green lines

Yu et al. [69] recently used genome-wide transcriptome profiling to study how *Bacillus subtilis* C232 lipopeptides inhibit microsclerotia formation in *Verticillium dahlia*. Lipopeptides inhibit the expression of genes associated with secondary metabolism, protein catabolism, and the high-osmolarity glycerol response signaling pathway. The results of the present study provided insights into the activation of genes responsible for the assimilation of fungal-derived compounds and the potential synthesis of an unverified antifungal agent. In addition, *B. safensis* MM19 produced various genes encoding protease and a gene encoding esterase/lipase (Supplementary Data S3). These bacterial enzymes could inhibit the cell wall of the pathogen by acting antagonistically. Because the cell membrane (plasma membrane, plasmalemma) of *P. viticola* involves a lipoprotein structure with a molecular organization that coincides with the principles of the fluid mosaic model [70], we conclude that these bacterial enzymes, and especially lipopeptides play role in antagonistic behavior.

Bacterial genes encoding products of similar adaptational functions are frequently coregulated (Fig. 6, Fig. 7). This organization ensures the balanced production of proteins necessary for adaptation to the antagonistic competition. Reorganization of the expression profile depending on signal transduction could be a featured case of competition between secreted metabolites by antagonist bacteria and stress factors affecting the pathogen, which limits its survival [71]. Further studies on integrated network models involving cellular behavior will enhance our profound understanding and knowledge of the correlation between genetic variations and metabolic pathways [72]. RNA-seq analysis is a key approach to determine the genes responsible for the responses of bacterium to various stress conditions resulting from abiotic and biotic sources. This technique presented in our study could pave the way for unveiling microbial behavior of each strain with antagonistic potential when it encounters a target pathogen, which could be used for further investigation.

Conclusion

This study investigated the whole gene expression profile of *B. safensis* MM19 during its interaction with *P. viticola* in liquid medium via RNA-seq analysis. The simultaneous application of several analysis methods (DEG analysis, KEGG analysis, K-mean cluster analysis, GO analysis, qPCR, network analysis, molecular docking involving dynamics simulation) allowed the expression patterns of genes and their functions to be revealed. High transcription level of the genes encoding the proteins linked to oxidoreductase and thiamine synthesis pathways signify the importance of possessing these genes for selecting the promising biocontrol agent candidate. Additionally, further studies on HOG1-thiamine interaction can extend our knowledge and enable us to design synthetic compounds mimicking thiamine targeting specific sides of the pathogen.

Supplementary Information The online version contains supplementary material available at https://doi.org/10.1007/s00284-024-03908-1.

Acknowledgements We are thankful to Assoc. Prof. Dr. Mustafa Küsek for Biolog Gen III analysis and Utku Berki Baysal (Junior computer engineer candidate) for Python coding support. The RNA-seq expression analysis of the whole raw data reads were also confirmed with Bacterial and Viral Bioinformatics Resource Center database (https://www.bv-brc.org) RNA-seq analysis pipeline.

Author Contributions RSS: Conceptualization, Data curation, Formal analysis, Funding acquisition, Investigation, Methodology, Project administration, Resources, Writing—original draft and Writing—review and editing. ÖB: Conceptualization, Data curation, Formal analysis, Investigation, Methodology, Resources, Software, Supervision, Validation, Visualization, Writing—original draft and Writing—review and editing. AC: Formal analysis, Methodology, Visualization. YK: Formal analysis, Methodology. AK: Formal analysis, Methodology, Visualization. KKK: Formal analysis, Methodology, Visualization. AÇ: Formal analysis, Methodology. All authors contributed to the article and approved the submitted version.

Funding The study has been supported by Istanbul University Scientific Research Projects Coordination Unit (Project Number: FBA-2019–33451).

Data Availability The datasets analyzed for this study can be found in the DNA Data Bank of Japan (http://trace.ddbj.nig.ac.jp/dra) under accession number SAMD00731600 (BioProject; PRJDB17356).

Code Availability Not applicable.

Declarations

Conflict of interest The authors declare that the research was conducted in the absence of any commercial or financial relationships that could be understood as a potential conflict of interest.

Ethical Approval Not applicable.

Consent to Participate Not applicable.

Consent for Publication Not applicable.

References

1. Raaijmakers JM, Vlami M, de Souza JT (2002) Antibiotic production by bacterial biocontrol agents. Antonie Van Leeuwenhoek 81:537–547. https://doi.org/10.1023/a:1020501420831
2. McSpadden Gardener BB (2004) Ecology of *Bacillus* and *Paenibacillus* spp. in agricultural systems. Phytopathology 94:1252–1258. https://doi.org/10.1094/PHYTO.2004.94.11.1252
3. Choudhary DK, Johri BN (2009) Interactions of *Bacillus* spp. and plants – With special reference to induced systemic resistance (ISR). Microbiol Res 164:493–513. https://doi.org/10.1016/j.micres.2008.08.007

4. Toure Y, Ongena M, Jacques P, Guiro A, Thonart P (2004) Role of lipopeptides produced by *Bacillus subtilis* GA1 in the reduction of grey mould disease caused by *Botrytis cinerea* on apple. J Appl Microbiol 96:1151–1160. https://doi.org/10.1111/j.1365-2672.2004.02252.x
5. Baysal Ö, Çalışkan M, Yeşilova Ö (2008) An inhibitory effect of a new *Bacillus subtilis* strain (EU07) against *Fusarium oxysporum* f. sp. *radicis-lycopersici*. Physiol Mol Plant Pathol 73:25–32. https://doi.org/10.1016/j.pmpp.2008.11.002
6. Baysal Ö, Lai D, Xu HH, Siragusa M, Çalışkan M, Carimi F, Teixeira da Silva JA, Tör M (2013) A proteomic approach provides new insights into the control of soil-borne plant pathogens by *Bacillus* species. PLoS ONE 8:e53182. https://doi.org/10.1371/journal.pone.0053182
7. Pandin C, Le Coq D, Canette A, Aymerich S, Briandet R (2017) Should the biofilm mode of life be taken into consideration for microbial biocontrol agents? Microb Biotechnol 10:719–734. https://doi.org/10.1111/1751-7915.12693
8. Miljaković D, Marinković J, Balešević-Tubić S (2020) The significance of Bacillus spp. in disease suppression and growth promotion of field and vegetable crops. Microorganisms 8:1037. https://doi.org/10.3390/microorganisms8071037
9. Satomi M, La Duc MT, Venkateswaran K (2006) *Bacillus safensis* sp. nov., isolated from spacecraft and assembly-facility surfaces. Int J Syst Evol Microbiol 56:1735–1740. https://doi.org/10.1099/ijs.0.64189-0
10. Tirumalai MR, Rastogi R, Zamani N, O'Bryant Williams E, Allen S, Diouf F, Kwende S, Weinstock GM, Venkateswaran KJ, Fox GE (2013) Candidate genes that may be responsible for the unusual resistances exhibited by *Bacillus pumilus* SAFR-032 spores. PLoS ONE 8:e66012. https://doi.org/10.1371/journal.pone.0066012
11. Chakraborty U, Chakraborty BN, Dey PL, Chakraborty AP (2018) *Bacillus safensis* from wheat rhizosphere promotes growth and ameliorates salinity stress in wheat. Indian J Biotechnol 17:466–479
12. Wu T, Xu J, Liu J, Guo WH, Li XB, Xia JB, Xie WJ, Yao ZG, Zhang YM, Wang RQ (2019) Characterization and initial application of endophytic *Bacillus safensis* strain ZY16 for improving phytoremediation of oil-contaminated saline soils. Front Microbiol 10:991. https://doi.org/10.3389/fmicb.2019.00991
13. Scheper RWA, Whisson DL, Scott ES (1997) Revised disease cycles of the two types of Phomopsis on grapevine. Aust J Grape Wine Res 9:41–44
14. van Niekerk JM, Halleen F, Fourie PH (2011) Temporal susceptibility of grapevine pruning wounds to trunk pathogen infection in South African grapevines. Phytopathol Mediterr 50:S139–S150
15. Castillo-Pando MS, Nair NG, Emmett RW, Wicks TJ (1997) Inhibition in pycnidial viability of *Phomopsis viticola* on canes in situ as an aid to reducing inoculum potential of cane and leaf blight disease of grapevines. Australas Plant Pathol 26:21–25. https://doi.org/10.1071/AP97003
16. Ramsdell DC (1995) Winter air-blast applications of benomyl for reduction of Eutypa dieback disease incidence in a Concord grape vineyard in Michigan. Plant Dis 79:399–405. https://doi.org/10.1094/PD-79-0399
17. Mostert L, Crous P (2000) Phomopsis (dead arm): new facets of this well-known vine disease. Wynboer 135:15–17
18. Munkvold GP, Marois JJ (1993) The effects of fungicides on *Eutypa lata* germination, growth and infection of grapevines. Plant Dis 77:50–55. https://doi.org/10.1094/PD-77-0050
19. Wolf T, Kämmer P, Brunke S, Linde J (2018) Two's company: studying interspecies relationships with dual RNA-seq. Curr Opin Microbiol 42:7–12. https://doi.org/10.1016/j.mib.2017.09.001
20. Chen S, Zhou Y, Chen Y, Gu J (2018) fastp: an ultra-fast all-in-one FASTQ preprocessor. Bioinformatics 34:i884–i890. https://doi.org/10.1093/bioinformatics/bty560
21. The Galaxy Community (2022) The Galaxy platform for accessible, reproducible and collaborative biomedical analyses: 2022 update. Nucleic Acids Res 50:W345–W351. https://doi.org/10.1093/nar/gkac247
22. Milne I, Stephen G, Bayer M, Cock PJ, Pritchard L, Cardle L, Shaw PD, Marshall D (2013) Using Tablet for visual exploration of second-generation sequencing data. Brief Bioinform 14:193–202. https://doi.org/10.1093/bib/bbs012
23. Ge SX, Son EW, Yao R (2018) iDEP: an integrated web application for differential expression and pathway analysis of RNA-Seq data. BMC Bioinform 19:534. https://doi.org/10.1186/s12859-018-2486-6
24. Conesa A, Götz S, García-Gómez JM, Terol J, Talón M, Robles M (2005) Blast2GO: a universal tool for annotation, visualization and analysis in functional genomics research. Bioinformatics 21:3674–3676. https://doi.org/10.1093/bioinformatics/bti610
25. Ge SX, Jung D, Yao R (2020) ShinyGO: a graphical gene-set enrichment tool for animals and plants. Bioinformatics 36:2628–2629. https://doi.org/10.1093/bioinformatics/btz931
26. Simple Real-Time Plotter (2013) https://sourceforge.net/projects/srtplot/. Accessed 15 June 2023
27. Reimand J, Isserlin R, Voisin V, Kucera M, Tannus-Lopes C, Rostamianfar A, Wadi L, Meyer M, Wong J, Xu C, Merico D, Bader GD (2019) Pathway enrichment analysis and visualization of omics data using g:Profiler, GSEA, Cytoscape and Enrichment Map. Nat Protoc 14:482–517. https://doi.org/10.1038/s41596-018-0103-9
28. Merico D, Isserlin R, Bader GD (2011) Visualizing gene-set enrichment results using the cytoscape plug-in enrichment map. In: Cagney G and Emili A (eds) Network Biology, Methods in Molecular Biology, Humana Press, pp 257–277. https://doi.org/10.1007/978-1-61779-276-2_12
29. Li S, Musungu B, Lightfoot D, Ji P (2018) The interactomic analysis reveals pathogenic protein networks in *Phomopsis longicolla* underlying seed decay of soybean. Front Genet 9:104. https://doi.org/10.3389/fgene.2018.00104
30. Du YC, Kong LJ, Cao LS, Zhang W, Zhu Q, Ma CY, Sun K, Dai CC (2022) Endophytic fungus *Phomopsis liquidambaris* enhances Fe absorption in peanuts by reducing hydrogen peroxide. Front Plant Sci 13:872242. https://doi.org/10.3389/fpls.2022.872242
31. Rozen S, Skaletsky H (2000) Primer3 on the WWW for general users and for biologist programmers. In: Misener S, Krawetz SA (eds) Bioinformatics Methods and Protocols. Methods in Molecular Biology, Humana Press, Totowa, NJ, pp 365–386
32. Pfaffl MW (2001) A new mathematical model for relative quantification in realtime RT–PCR. Nucleic Acids Res 29:e45. https://doi.org/10.1093/nar/29.9.e45
33. Wilson KP, Fitzgibbon MJ, Caron PR, Griffith JP, Chen W, McCaffrey PG, Chambers SP, Su MS (1996) Crystal structure of p38 mitogen-activated protein kinase. J Biol Chem 271:27696–27700. https://doi.org/10.1074/jbc.271.44.27696
34. Berman H, Henrick K, Nakamura H (2003) Announcing the worldwide Protein Data Bank. Nat Struct Mol Biol 10:980. https://doi.org/10.1038/nsb1203-980
35. Webb B, Sali A (2016) Comparative Protein Structure Modeling Using MODELLER. Curr Protoc Bioinformatics 54:5.6.1–5.6.37. https://doi.org/10.1002/cpbi.3
36. Fiser A, Do RK, Sali A (2000) Modeling of loops in protein structures. Protein Sci 9:1753–1773. https://doi.org/10.1110/ps.9.9.1753

37. The PyMOL Molecular Graphics System. Version 2.5.0. Schrödinger, LLC. (2023) https://pymol.org/2/. Accessed 15 June 2023
38. Morris GM, Huey R, Lindstrom W, Sanner MF, Belew RK, Goodsell DS, Olson AJ (2009) AutoDock4 and AutoDockTools4: automated docking with selective receptor flexibility. J Comput Chem 30:2785–2791. https://doi.org/10.1002/jcc.21256
39. Trott O, Olson AJ (2010) AutoDock Vina: improving the speed and accuracy of docking with a new scoring function, efficient optimization, and multithreading. J Comput Chem 31:455–461. https://doi.org/10.1002/jcc.21334
40. Salentin S, Schreiber S, Haupt VJ, Adasme MF, Schroeder M (2015) PLIP: fully automated protein-ligand interaction profiler. Nucleic Acids Res 43:W443–W447. https://doi.org/10.1093/nar/gkv315
41. Ahamad S, Hassan MI, Dwivedi N (2018) Designing of phenol-based β−carbonic anhydrase1 inhibitors through QSAR, molecular docking, and M.D. simulation approach. Biotech 8:256. https://doi.org/10.1007/s13205-018-1278-z
42. Ahamad S, Kanipakam H, Birla S, Ali MS, Gupta D (2021) Screening Malaria-box compounds to identify potential inhibitors against SARS-CoV-2 Mpro, using molecular docking and dynamics simulation studies. Eur J Pharmacol 890:173664. https://doi.org/10.1016/j.ejphar.2020.173664
43. Schrödinger Release 2022–3: Maestro. New York (2021) https://www.schrodinger.com/products/maestro. Accessed 15 June 2023
44. Coppins RL, Hall KB, Groisman EA (2007) The intricate world of riboswitches. Curr Opin Microbiol 10:176–181. https://doi.org/10.1016/j.mib.2007.03.006
45. Roth A, Breaker RR (2009) The structural and functional diversity of metabolite-binding riboswitches. Annu Rev Biochem 78:305–334. https://doi.org/10.1146/annurev.biochem.78.070507.135656
46. Kubodera T, Watanabe M, Yoshiuchi K, Yamashita N, Nishimura A, Nakai S, Gomi K, Hanamoto H (2003) Thiamine-regulated gene expression of *Aspergillus oryzae* thiA requires splicing of the intron containing a riboswitch-like domain in the 5'-UTR. FEBS Lett 555:516–520. https://doi.org/10.1016/S0014-5793(03)01335-8
47. Kazanov MD, Vitreschak AG, Gelfand MS (2007) Abundance and functional diversity of riboswitches in microbial communities. BMC Genom 8:347. https://doi.org/10.1186/1471-2164-8-347
48. Schyns G, Potot S, Geng Y, Barbosa TM, Henriques A, Perkins JB (2005) Isolation and characterization of new thiamine-deregulated mutants of *Bacillus subtilis*. J Bacteriol 187:8127–8136. https://doi.org/10.1128/JB.187.23.8127-8136.2005
49. Younus H (2019) Oxidoreductases: Overview and Practical Applications. In: Husain Q, Ullah M (eds) Biocatalysis. Springer, Cham, pp 39–55
50. Paul PEV, Sangeetha V, Deepika RG (2019) Chapter 9 - Emerging Trends in the Industrial Production of Chemical Products by Microorganisms. In: Buddolla V (ed) Recent Developments in Applied Microbiology and Biochemistry. Academic Press, pp 107–125
51. Jiang L, Ma Q, Li A, Sun R, Tang G, Huang X, Pu H (2023) Bioactive secondary metabolites produced by fungi of the genus Diaporthe (*Phomopsis*): Structures, biological activities, and biosynthesis. Arab J Chem 16:105062. https://doi.org/10.1016/j.arabjc.2023.105062
52. McCormick SP, Stanley AM, Stover NA, Alexander NJ (2011) Trichothecenes: from simple to complex mycotoxins. Toxins (Basel) 3:802–814. https://doi.org/10.3390/toxins3070802
53. Mostrom MS, Raisbeck MF (2007) CHAPTER 76 – Trichothecenes. In: Gupta RC (ed) Veterinary Toxicology. Academic Press, pp 951–976
54. Afsharmanesh H, Perez-Garcia A, Zeriouh H, Ahmadzadeh M, Romero D (2018) Aflatoxin degradation by *Bacillus subtilis* UTB1 is based on production of an oxidoreductase involved in bacilysin biosynthesis. Food Control 94:48–55. https://doi.org/10.1016/j.foodcont.2018.03.002
55. Hwang S, Cordova B, Abdo M, Pfeiffer F, Maupin-Furlow JA (2017) ThiN as a versatile domain of transcriptional repressors and catalytic enzymes of thiamine biosynthesis. J Bacteriol 199:e00810–e00816. https://doi.org/10.1128/JB.00810-16
56. Chen Y, Wang L, Shang F, Liu W, Lan J, Chen J, Ha NC, Quan C, Nam KH, Xu Y (2019) Structural insight of the 5-(Hydroxyethyl)-methylthiazole kinase ThiM involving vitamin B1 biosynthetic pathway from the *Klebsiella pneumoniae*. Biochem Biophys Res Commun 518:513–518. https://doi.org/10.1016/j.bbrc.2019.08.086
57. Schauer K, Stolz J, Scherer S, Fuchs TM (2009) Both thiamine uptake and biosynthesis of thiamine precursors are required for intracellular replication of *Listeria monocytogenes*. J Bacteriol 191:2218–2227. https://doi.org/10.1128/JB.01636-08
58. Yu X, Liang X, Liu K, Dong W, Wang J, Zhou M (2015) The thiG gene is required for full virulence of Xanthomonas oryzae pv. oryzae by preventing cell aggregation. PLoS ONE 10:e0134237. https://doi.org/10.1371/journal.pone.0134237
59. Madeo M, O'Riordan N, Fuchs TM, Utratna M, Karatzas KAG, O'Byrne CP (2012) Thiamine plays a critical role in the acid tolerance of *Listeria monocytogenes*. FEMS Microbiol Lett 326:137–143. https://doi.org/10.1111/j.1574-6968.2011.02442.x
60. Liu J, Zhang X, Deng S, Wang H, Zhao Y (2022) Thiamine is required for virulence and survival of Pseudomonas syringae pv. tomato DC3000 on tomatoes. Front Microbiol 13:903258. https://doi.org/10.3389/fmicb.2022.903258
61. Morrison DK (2012) MAP kinase pathways. Cold Spring Harb Perspect Biol 4:a011254. https://doi.org/10.1101/cshperspect.a011254
62. Brewster JL, Gustin MC (2014) Hog 1: 20 years of discovery and impact. Sci Signal. https://doi.org/10.1126/scisignal.2005458
63. Mody A, Weiner J, Ramanathan S (2009) Modularity of MAP kinases allows deformation of their signalling pathways. Nat Cell Biol 11:484–491. https://doi.org/10.1038/ncb1856
64. Siemieniuk M, Czyzewska U, Strumilo S, Tylicki A (2016) Thiamine antivitamins – an opportunity of therapy of fungal infections caused by *Malassezia pachydermatis* and *Candida albicans*. Mycoses 59:108–116. https://doi.org/10.1111/myc.12441
65. Bettendorff L, Wins P (2013) Biological functions of thiamine derivatives: focus on non-coenzyme roles. OA Biochem 1:10
66. Gigliobianco T, Lakaye B, Wins P, El Moualij B, Zorzi W, Bettendorff L (2010) Adenosine thiamine triphosphate accumulates in *Escherichia coli* cells in response to specific conditions of metabolic stress. BMC Microbiol 10:148. https://doi.org/10.1186/1471-2180-10-148
67. Nabokina SM, Inoue K, Subramanian VS, Valle JE, Yuasa H, Said HM (2014) Molecular identification and functional characterization of the human colonic thiamine pyrophosphate transporter. J Biol Chem 289:4405–4416. https://doi.org/10.1074/jbc.M113.528257
68. Tanaka T, Yamamoto D, Sato T, Tanaka S, Usui K, Manabe M, Aoki Y, Iwashima Y, Saito Y, Mino Y, Deguchi H (2011) Adenosine thiamine triphosphate (AThTP) inhibits poly (ADP-ribose) polymerase-1 (PARP-1) activity. J Nutr Sci Vitaminol 57:192–196. https://doi.org/10.3177/jnsv.57.192
69. Yu D, Fang Y, Tang C, Klosterman SJ, Tian C, Wang Y (2019) Genomewide transcriptome profiles reveal how *Bacillus subtilis* lipopeptides inhibit microsclerotia formation in *Verticillium dahliae*. Mol Plant Microbe Interact 32:622–634. https://doi.org/10.1094/MPMI-08-18-0233-R
70. Coppin E, Debuchy R, Arnaise S, Picard M (1997) Mating types and sexual development in filamentous ascomycetes. Microbiol

Mol Biol Rev 61:411–428. https://doi.org/10.1128/mmbr.61.4.411-428.1997

71. Seshasayee AS, Bertone P, Fraser GM, Luscombe NM (2006) Transcriptional regulatory networks in bacteria: from input signals to output responses. Curr Opin Microbiol 9:511–519. https://doi.org/10.1016/j.mib.2006.08.007
72. Goelzer A, Bekkal Brikci F, Martin-Verstraete I, Noirot P, Bessières P, Aymerich S, Fromion V (2008) Reconstruction and analysis of the genetic and metabolic regulatory networks of the central metabolism of *Bacillus subtilis*. BMC Syst Biol 2:20. https://doi.org/10.1186/1752-0509-2-20